ELSEVIER

Engineering Analysis with Boundary Elements 31 (2007) 683–691

ENGINEERING ANALYSIS with BOUNDARY ELEMENTS

www.elsevier.com/locate/enganabound

Efficient and accurate multi-layered elastostatic Green's functions via the bi-material Green's function

Jiandong Xu[a], Trevor G. Davies[a,*], Ernian Pan[b]

[a]*Department of Civil Engineering, Glasgow University, Glasgow G12 8QQ, UK*
[b]*Department of Civil Engineering, Akron University, Akron, OH 44325, USA*

Received 20 September 2006; accepted 12 December 2006
Available online 12 March 2007

Abstract

The three-dimensional elastostatic Green's functions for multi-layered half-spaces are expressed in terms of a cylindrical system of vector functions using the propagator matrix method. To obtain efficient and accurate results near the singularity at the interface between layers, the singularity extraction method is employed in the transform domain, based on the singular solutions for the bi-material full space expressed here in vector cylindrical function form. Numerical trials demonstrate that this approach improves on previous work, which relied on singularity extraction based on the well-known singular (Kelvin) solution for the homogenous full-space. A boundary element implementation illustrates the practical potential of this work to boundary value problems.

Keywords: Green's function; Multi-layer; Bi-material; Boundary element

1. Introduction

Multi-layered solids occur commonly in nature and in man-made artefacts (e.g., geological strata, roads, composites, biological tissue, etc.). However, efficient stress analysis of these materials by means of integral methods is stymied by the lack of suitable Green's functions. The principal difficulty is that whereas the Green's functions for homogeneous media can be expressed in closed form, those for multi-layered media must themselves be integrated numerically. Devising efficient integration strategies is therefore central to the problem.

For horizontally infinite and layered systems, Green's functions can be derived using the propagator matrix method, which originates in the work of Thomson [1], Haskell [2], and Gilbert and Backus [3] in elasto-dynamics. More recent work is described in [4–7]. For the elastostatic problem, the propagator matrix can be obtained directly rather than as a special case of elastodynamics. Solutions for multi-layered isotropic media have been obtained by Singh [8], Jovanovich et al. [9], Sato and Matsu'ura [10], Singh [11] and Yue and Wang [12] for transversely isotropic media. The special case of a finite layer underlain by a half-space was solved by Chan et al. [13]. Pan [14–16] employed a novel cylindrical system of vector functions to derive elastostatic Green's functions for multi-layered transversely isotropic half spaces. Parallel work using a Stroh formulation has been reported by Yuan and Yang [17] and Yang and Pan [18,19]. The numerical computation of these Green's function solutions is difficult.

In this paper, we describe an efficient and robust approach for accurate calculation of the multilayered Green's functions in isotropic media. It employs a singularity extraction approach in the multi-layered Green's functions using the analytical bi-material Green's function solution. A similar method of attack, but in the context of wave motions and differing in significant detail, has been reported independently by Guzina and Pak [20]. The paper is organized as follows: in Section 2, we review briefly the basic equations in terms of the cylindrical system of vector functions. In Section 3, the layered Green's functions are presented. The singularity extraction issue is discussed in Section 4, and the bi-material Green's functions are

*Corresponding author. Tel.: +44 141 330 4077; fax: +44 141 330 4557.
E-mail address: davies@civil.gla.ac.uk (T.G. Davies).

0955-7997/$ - see front matter © 2007 Elsevier Ltd. All rights reserved.
doi:10.1016/j.enganabound.2006.12.006

presented in Section 5. In Section 6, we demonstrate the efficiency and accuracy of the method and illustrate its implementation in a boundary element analysis.

2. Basic relations in terms of the cylindrical system of vector functions

We consider a system of linearly elastic isotropic parallel layers, which are fully bonded at their interfaces. The horizontal variables of a (horizontally) layered system can be suppressed using a Fourier or Hankel transformation of the governing equations, which leads to a set of more tractable first-order differential equations. The (transformed) solutions are functions of the vertical variable z only. However, a transformation using a cylindrical system of vector functions [14,15] offers greater generality. The cylindrical system of vector functions is defined as

$$\begin{aligned}
\boldsymbol{L}(r,\theta;\lambda,m) &= \boldsymbol{i}_z S(r,\theta;\lambda,m),\\
\boldsymbol{M}(r,\theta;\lambda,m) &= \left(\boldsymbol{i}_r\frac{\partial}{\partial r}+\boldsymbol{i}_\theta\frac{\partial}{r\partial\theta}\right)S(r,\theta;\lambda,m),\\
\boldsymbol{N}(r,\theta;\lambda,m) &= \left(\boldsymbol{i}_r\frac{\partial}{r\partial\theta}-\boldsymbol{i}_\theta\frac{\partial}{\partial r}\right)S(r,\theta;\lambda,m),
\end{aligned}\tag{1}$$

where λ is the transform parameter and

$$S(r,\theta;\lambda,m)=\frac{1}{\sqrt{2\pi}}J_m(\lambda r)\mathrm{e}^{\mathrm{i}m\theta},\tag{2}$$

where $\mathrm{i}=\sqrt{-1}$, $J_m(\lambda r)$ is the Bessel function of order m, and $\boldsymbol{i}_r,\boldsymbol{i}_\theta,\boldsymbol{i}_z$ are the unit vectors in the radial, angular and vertical directions, respectively (Fig. 1).

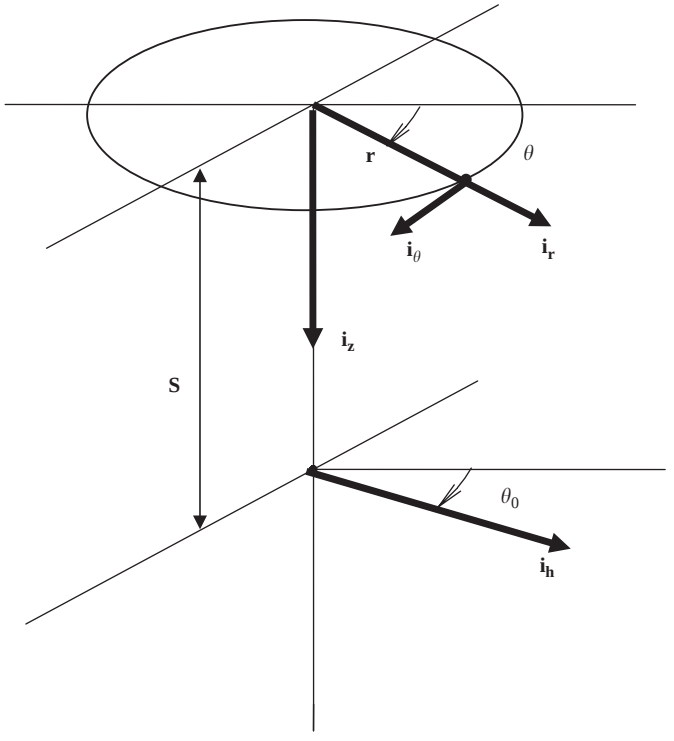

Fig. 1. Orientation of point loads.

Since this system forms an orthogonal and complete space, the displacement and traction vectors can be expressed in the form [14]:

$$\begin{aligned}
\boldsymbol{u}(r,\theta,z) &= \sum_m\int_0^\infty [U_L(z)\boldsymbol{L}(r,\theta)+U_M(z)\boldsymbol{M}(r,\theta)\\
&\quad + U_N(z)\boldsymbol{N}(r,\theta)]\lambda\,\mathrm{d}\lambda,\\
\boldsymbol{t}(r,\theta,z) &= \sigma_{rz}\boldsymbol{i}_r+\sigma_{\theta z}\boldsymbol{i}_\theta+\sigma_{zz}\boldsymbol{i}_z\\
&= \sum_m\int_0^\infty [T_L(z)\boldsymbol{L}(r,\theta)+T_M(z)\boldsymbol{M}(r,\theta)\\
&\quad + T_N(z)\boldsymbol{N}(r,\theta)]\lambda\,\mathrm{d}\lambda,
\end{aligned}\tag{3}$$

where $U_L(z), U_M(z), U_N(z)$ are the transformed displacement coefficients in the cylindrical system, and $T_L(z), T_M(z), T_N(z)$ are the transformed traction coefficients.

Without loss of generality, the horizontal and vertical unit point loads may be assumed to act at a depth $z=s$ on the z-axis, i.e.

$$\begin{aligned}
\boldsymbol{f}_h(r,\theta,z) &= \frac{1}{2\pi r}\delta(r)\delta(z-s)\boldsymbol{i}_h,\\
\boldsymbol{f}_z(r,\theta,z) &= \frac{1}{2\pi r}\delta(r)\delta(z-s)\boldsymbol{i}_z,
\end{aligned}\tag{4}$$

where δ is the Dirac delta function and $\boldsymbol{i}_h$ is the horizontal unit vector in the $\theta=\theta_0$ direction (Fig. 1). We thus have

$$\boldsymbol{i}_h = n_r\boldsymbol{i}_r+n_\theta\boldsymbol{i}_\theta=\cos(\theta-\theta_0)\boldsymbol{i}_r-\sin(\theta-\theta_0)\boldsymbol{i}_\theta,\tag{5}$$

where n_r, n_θ are the direction cosines of the unit force vector.

In general, a body force can be expressed in the form:

$$\begin{aligned}
\boldsymbol{f}(r,\theta,z) &= f_h\cdot\boldsymbol{i}_h+f_z\cdot\boldsymbol{i}_z\\
&= \sum_m\int_0^{+\infty}[F_L(z)\boldsymbol{L}(r,\theta)+F_M(z)\boldsymbol{M}(r,\theta)\\
&\quad + F_N(z)\boldsymbol{N}(r,\theta)\lambda\,\mathrm{d}\lambda,
\end{aligned}\tag{6}$$

where the transformed body force coefficients are [15]

$$\begin{aligned}
F_L &= \int_0^{2\pi}\int_0^{+\infty}\boldsymbol{f}\cdot\boldsymbol{L}^*(r,\theta)r\,\mathrm{d}r\,\mathrm{d}\theta,\\
F_M &= \lambda^{-2}\int_0^{2\pi}\int_0^{+\infty}\boldsymbol{f}\cdot\boldsymbol{M}^*(r,\theta)r\,\mathrm{d}r\,\mathrm{d}\theta,\\
F_N &= \lambda^{-2}\int_0^{2\pi}\int_0^{+\infty}\boldsymbol{f}\cdot\boldsymbol{N}^*(r,\theta)r\,\mathrm{d}r\,\mathrm{d}\theta,
\end{aligned}\tag{7}$$

where the asterisk indicates the complex conjugate. For the concentrated unit body force expressed by Eq. (4), the transformed body force coefficients can be obtained by substituting Eq. (6) into Eq. (7). We thus obtain

$$\begin{aligned}
F_L &= \frac{n_z}{\sqrt{2\pi}} \quad m=0,\\
F_M &= \frac{\pm\mathrm{e}^{\mp\mathrm{i}\theta_0}}{2\lambda\sqrt{2\pi}} \quad m=\pm1,\\
F_N &= \frac{-\mathrm{i}\mathrm{e}^{\mp\mathrm{i}\theta_0}}{2\lambda\sqrt{2\pi}} \quad m=\pm1.
\end{aligned}\tag{8}$$

It can be shown [15] that the point force vector yields the following discontinuities in the expansion coefficients of the traction vector, namely

$$\begin{aligned} T_L(s-) - T_L(s+) &= \frac{n_z}{\sqrt{2\pi}} \qquad m = 0, \\ T_M(s-) - T_M(s+) &= \frac{\pm e^{\mp i\theta_0}}{2\lambda\sqrt{2\pi}} \quad m = \pm 1, \\ T_N(s-) - T_N(s+) &= \frac{-ie^{\mp i\theta_0}}{2\lambda\sqrt{2\pi}} \quad m = \pm 1. \end{aligned} \tag{9}$$

Substituting Eq. (3) into the equations of equilibrium and the constitutive relations, two independent sets of simultaneous linear differential equations for U_L, U_M, T_L, T_M, and U_N, T_N, are obtained. Details of the solution of these equations can be found in Pan [14,15] based on the propagator matrix method, but we briefly list some of the Green's functions here to clarify the following discussion.

3. Green's functions for multi-layered half-spaces

The Green's functions in terms of cylindrical coordinates assume the following general form in each layer (in which it is understood that the right-hand sides are to be multiplied by λ and integrated from zero to infinity with respect to λ)

$$\begin{aligned} u_r = {} & \frac{U_{M-1}(z)}{\sqrt{2\pi}}[J_1(\lambda r)/r - \lambda J_0(\lambda r)]e^{-i\theta} \\ & + \frac{U_{N-1}(z)}{\sqrt{2\pi}} i\frac{J_1(\lambda r)}{r} e^{-i\theta} \\ & + \frac{U_{M+1}(z)}{\sqrt{2\pi}}[\lambda J_0(\lambda r) - J_1(\lambda r)/r]e^{i\theta} \\ & + \frac{U_{N+1}(z)}{\sqrt{2\pi}} i\frac{J_1(\lambda r)}{r} e^{i\theta} - \frac{U_{M0}(z)}{\sqrt{2\pi}}\lambda J_1(\lambda r) \\ u_\theta = {} & \frac{U_{M-1}(z)}{\sqrt{2\pi}} i\frac{J_1(\lambda r)}{r} e^{-i\theta} \\ & - \frac{U_{N-1}(z)}{\sqrt{2\pi}}[J_1(\lambda r)/r - \lambda J_0(\lambda r)]e^{-i\theta} \\ & + \frac{U_{M+1}(z)}{\sqrt{2\pi}} i\frac{J_1(\lambda r)}{r} e^{i\theta} \\ & - \frac{U_{N+1}(z)}{\sqrt{2\pi}}[\lambda J_0(\lambda r) - J_1(\lambda r)/r]e^{i\theta} + \frac{U_{N0}(z)}{\sqrt{2\pi}}\lambda J_1(\lambda r), \\ u_z = {} & -\frac{U_{L-1}(z)}{\sqrt{2\pi}} J_1(\lambda r)e^{-i\theta} + \frac{U_{L+1}(z)}{\sqrt{2\pi}} J_1(\lambda r)e^{i\theta} \\ & + \frac{U_{L0}(z)}{\sqrt{2\pi}} J_0(\lambda r). \end{aligned} \tag{10}$$

Adopting the same convention, the corresponding tractions on the horizontal plane are

$$\begin{aligned} \sigma_{rz} = {} & \frac{T_{M-1}(z)}{\sqrt{2\pi}}[J_1(\lambda r)/r - \lambda J_0(\lambda r)]e^{-i\theta} \\ & + \frac{T_{N-1}(z)}{\sqrt{2\pi}} i\frac{J_1(\lambda r)}{r} e^{-i\theta} + \frac{T_{M+1}(z)}{\sqrt{2\pi}}[\lambda J_0(\lambda r) - J_1(\lambda r)/r]e^{i\theta} \\ & + \frac{T_{N+1}(z)}{\sqrt{2\pi}} i\frac{J_1(\lambda r)}{r} e^{i\theta} - \frac{T_{M0}(z)}{\sqrt{2\pi}}\lambda J_1(\lambda r) \\ \sigma_{\theta z} = {} & \frac{T_{M-1}(z)}{\sqrt{2\pi}} i\frac{J_1(\lambda r)}{r} e^{-i\theta} - \frac{T_{N-1}(z)}{\sqrt{2\pi}}[J_1(\lambda r)/r - \lambda J_0(\lambda r)]e^{-i\theta} \\ & + \frac{T_{M+1}(z)}{\sqrt{2\pi}} i\frac{J_1(\lambda r)}{r} e^{i\theta} - \frac{T_{N+1}(z)}{\sqrt{2\pi}}[\lambda J_0(\lambda r) - J_1(\lambda r)/r]e^{i\theta} \\ & + \frac{T_{N0}(z)}{\sqrt{2\pi}}\lambda J_1(\lambda r), \\ \sigma_{zz} = {} & -\frac{T_{L-1}(z)}{\sqrt{2\pi}} J_1(\lambda r)e^{-i\theta} + \frac{T_{L+1}(z)}{\sqrt{2\pi}} J_1(\lambda r)e^{i\theta} + \frac{T_{L0}(z)}{\sqrt{2\pi}} J_0(\lambda r). \end{aligned} \tag{11}$$

We remark that the remaining stress components can be obtained from Hooke's law from these displacements and tractions. It is further noted that all of these integrands are oscillatory (arising from the Bessel functions) and their convergence characteristics vary across a wide spectrum. Following Pan [14], we make use of an adaptive Gauss quadrature, developed by Patterson [21,22] and implemented by Chave [23], to compute these integrals. First, the infinite integrals are expressed as a finite sum

$$\int_0^\infty f(\lambda, z)J_m(\lambda r)\,d\lambda \approx \sum_{n=1}^{N}\int_{\lambda_n}^{\lambda_{n+1}} f(\lambda, z)J_m(\lambda r)\,d\lambda, \tag{12}$$

where $f(\lambda,z)$ represents any one of the expansion coefficients in the transformed domain and, in general, the product $\lambda_n r$ is the nth zero of the Bessel function. Then, in each sub-interval of integration, a first estimate is obtained using three-point Gauss quadrature

$$\int_{\lambda_n}^{\lambda_{n+1}} f(\lambda, z)J_m(\lambda r)\,d\lambda \approx \sum_{i=1}^{3} w_i f(\lambda_i, z)J_m(\lambda_i r), \tag{13}$$

where λ_i is the abscissa and w_i is the weight. Using Patterson's algorithm, new Gauss points are added into the interval between the existing Gauss points until the convergence criterion is satisfied. For slowly convergent integrals, a continued fraction expansion method [14,24] is employed to accelerate convergence.

4. Singularity extraction

Gauss quadrature becomes increasingly ineffective at the near-singularities, which arise when displacements and stresses are computed in the vicinity of the point load. But this is precisely where the greatest accuracy is required in practice. The general technique of singularity extraction may be applied here, namely

$$\begin{aligned} \int_0^\infty f(\lambda, z)J_m(\lambda r)\,d\lambda = {} & \int_0^\infty [f(\lambda, z) - g(\lambda, z)]J_m(\lambda r)\,d\lambda \\ & + \int_0^\infty g(\lambda, z)J_m(\lambda r)\,d\lambda, \end{aligned} \tag{14}$$

where $g(\lambda,z)$ is the singular part of the function $f(\lambda,z)$ and is integrable by analytical methods. The first integral on the RHS is evidently non-singular and is therefore integrable

by numerical quadrature. Here, the second integral on the RHS is that part of the corresponding full-space Green's function (e.g., Kelvin's solution) in the physical domain. Evidently, its transform $g(\lambda,z)$ must also be determined. For the transversely isotropic case, these can be derived using the solution by Pan and Chou [25]. However, when the singularity is at a layer interface, the analytical Green's functions for homogenous materials (e.g., Kelvin's solution) fail to capture the singularity. In these cases, singularity extraction can be effective only if the singular solution for a bi-material is used. Green's functions for a bi-material full-space have been obtained by Yue [26] and Guzina and Pak [27] in closed form. However, we also need the corresponding functions in the transform domain, and these are presented below.

5. Bi-material Green's functions in the transformed domain

The physical domain is assumed to be composed of two dis-similar isotropic elastic half spaces which are fully bonded across the plane $z = 0$ (Fig. 2). The Lame constants of the upper and lower half-spaces, denoted by (λ_1, μ_1) and (λ_2, μ_2), respectively, are used inter-changeably with Young's modulus E and Poisson's ratio v, for clarity.

Without loss of generality, it is assumed that the loaded plane is located in the lower half-space, i.e., $s>0$. Further, the lower half space is comprised of two parts; Region 2 ($0<z<s$) and Region 3 ($z>s$). From the inter-regional

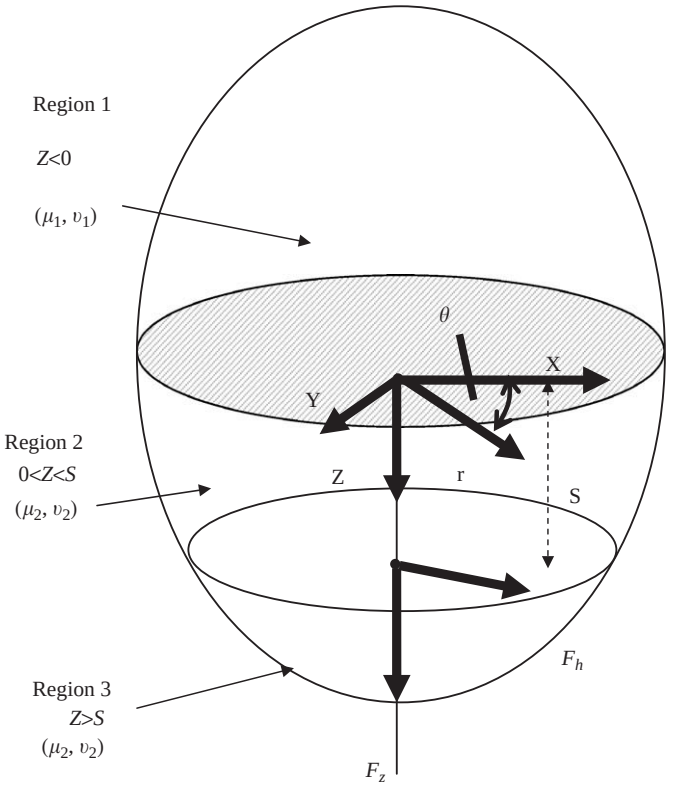

Fig. 2. The bi-material full-space.

equilibrium and compatibility conditions, we obtain 12 equations, which are sufficient to determine the 12 unknown coefficients in the transformed domain. After some algebra [28], the resulting Green's functions in the transformed domain may be determined (below). These are found to agree, within a scalar constant, with the auxiliary functions obtained by Guzina and Pak [27]. As usual, to determine the corresponding functions in the physical domain, the integral with respect to λ, over the limits from zero to infinity of the product of these expressions with λ, must be computed.

For Region 1:

$$
\begin{aligned}
U_{N0}(z) &= 0,\\
T_{N0}(z)/\lambda &= 0,\\
U_{L0}(z) &= \frac{F_{L0}\exp(-\lambda d_1)}{2\lambda M_1 M_2}[2\mu_1(3-4v_2)(1-v_1)\\
&\quad + 2\mu_2(3-4v_1)(1-v_2)+\lambda(sM_1-zM_2)],\\
\lambda U_{M0}(z) &= \frac{F_{L0}\exp(-\lambda d_1)}{2\lambda M_1 M_2]}[-\mu_1(3-4v_2)(1-2v_1)\\
&\quad + \mu_2(3-4v_1)(1-2v_2)+\lambda(sM_1-zM_2)],\\
T_{L0}(z)/\lambda &= \frac{\mu_1 F_{L0}\exp(-\lambda d_1)}{2\lambda M_1 M_2}[M_1(3-4v_2)+M_2\\
&\quad + 2\lambda(sM_1-zM_2)],\\
T_{M0}(z) &= \frac{\mu_1 F_{L0}\exp(-\lambda d_1)}{2\lambda M_1 M_2}[\mu_2(3-4v_1)(3-4v_2)\\
&\quad - \mu_2 + 2\lambda(sM_1-zM_2)],
\end{aligned}
\tag{15}
$$

where the second subscript "0" denotes order $m = 0$ in the vector function expansion. This convention is adopted in other expressions presented below.

$$
\begin{aligned}
U_{N1}(z) &= \frac{F_{N1}\exp(-\lambda d_1)}{\lambda(\mu_1+\mu_2)},\\
T_{N1}(z)/\lambda &= \frac{\mu_1 F_{L1}\exp(-\lambda d_1)}{\lambda(\mu_1+\mu_2)},\\
U_{L1}(z) &= \frac{F_{M1}\exp(-\lambda d_1)}{4M_1 M_2}[M_1(3-4v_2)\\
&\quad - M_2(3-4v_1)+2\lambda(zM_2-sM_1)],\\
\lambda U_{M1}(z) &= \frac{F_{M1}\exp(-\lambda d_1)}{4M_1 M_2}[M_1(3-4v_2)\\
&\quad + M_2(3-4v_1)+2\lambda(zM_2-sM_1)],\\
T_{L1}(z)/\lambda &= \frac{\mu_1 F_{M1}\exp(-\lambda d_1)}{2M_1 M_2}[M_1(3-4v_2)\\
&\quad - M_2 + 2\lambda(zM_2-sM_1)],\\
T_{M1}(z) &= \frac{\mu_1 F_{M1}\exp(-\lambda d_1)}{2M_1 M_2}[M_1(3-4v_2)\\
&\quad + M_2 + 2\lambda(zM_2-sM_1)],
\end{aligned}
\tag{16}
$$

$$
\begin{aligned}
d_1 &= |z-s|,\\
d_2 &= z+s,\\
d_3 &= z-s,
\end{aligned}
$$

$$M_1 = \mu_1 + (3-4\nu_1)\mu_2,$$
$$M_2 = \mu_2 + (3-4\nu_2)\mu_1. \tag{17}$$

For Region 2 and 3:

$$U_{N0}(z) = 0,$$
$$T_{N0}(z)/\lambda = 0,$$
$$\begin{aligned} U_{L0}(z) = {} & \frac{F_{L0}\exp(-\lambda d_1)}{8\mu_2\lambda(1-\nu_2)}(3-4\nu_2+\lambda d_1) \\ & + \frac{F_{L0}\exp(-\lambda d_2)}{8\mu_2\lambda M_1 M_2(1-\nu_2)} \\ & [-2\lambda^2(\mu_1-\mu_2)M_1 zs - M_1(\mu_1 \\ & - \mu_2)(3-4\nu_2)\lambda d_2 - (\mu_1^2(3-4\nu_2)^2 \\ & - \mu_2^2(3-4\nu_1)(5-12\nu_2+8\nu_2^2) \\ & + \mu_1\mu_2(3-4\nu_2)(2-4\nu_1)(1-2\nu_2))], \\ \lambda U_{M0}(z) = {} & \frac{-F_{L0}\exp(-\lambda d_1)}{8\mu_2(1-\nu_2)}d_3 \\ & + \frac{F_{L0}\exp(-\lambda d_2)}{8\mu_2\lambda M_1 M_2(1-\nu_2)}[-4\mu_2(1-\nu_2) \\ & (\mu_1(3-4\nu_2)(1-2\nu_1) - \mu_2(3-4\nu_1)(1-2\nu_2)) \\ & + M_1(\mu_1-\mu_2)(3-4\nu_2)\lambda d_3 \\ & + 2\lambda^2(\mu_1-\mu_2)M_1 sz], \end{aligned} \tag{18}$$

$$\begin{aligned} T_{L0}(z)/\lambda = {} & \frac{-F_{L0}\exp(-\lambda d_1)}{4\lambda(1-\nu_2)}\mathrm{sign}(z-s)(2-2\nu_2+\lambda d_1) \\ & + \frac{F_{L0}\exp(-\lambda d_2)}{4\lambda M_1 M_2(1-\nu_2)}[2\mu_1^2(3-4\nu_2)(1-\nu_2) \\ & - 2\mu_2^2(3-4\nu_1)(1-\nu_2) + \lambda s M_1(\mu_1-\mu_2) \\ & + \lambda z M_1(\mu_1-\mu_2)(3-4\nu_2) \\ & + 2\lambda^2(\mu_1-\mu_2)M_1 sz)], \\ T_{M0}(z) = {} & \frac{F_{L0}\exp(-\lambda d_1)}{4\lambda(1-\nu_2)}(1-2\nu_2+\lambda d_1) \\ & + \frac{F_{L0}\exp(-\lambda d_2)}{4\lambda M_1 M_2(1-\nu_2)}[2\mu_1\mu_2(3-4\nu_2)(1-2\nu_1) \\ & - \mu_1^2(3-4\nu_2)(1-2\nu_2) - \mu_2^2(3-4\nu_1)(1-2\nu_2) \\ & + \lambda s M_1(\mu_1-\mu_2) - \lambda s M_1(\mu_1-\mu_2)(3-4\nu_2) \\ & - 2\lambda^2(\mu_1-\mu_2)M_1 sz]. \end{aligned}$$

And

$$U_{N1}(z) = \frac{F_{N1}\exp(-\lambda d_1)}{2\mu_2\lambda} - \frac{F_{N1}\exp(-\lambda d_2)(\mu_1-\mu_2)}{2\mu_2\lambda(\mu_1+\mu_2)},$$
$$T_{N1}(z)/\lambda = -\frac{F_{L1}\exp(-\lambda d_1)}{2\lambda}\mathrm{sign}(z-s) + \frac{F_{N1}\exp(-\lambda d_2)(\mu_1-\mu_2)}{2\lambda(\mu_1+\mu_2)},$$

$$\begin{aligned} U_{L1}(z) = {} & \frac{F_{M1}\exp(-\lambda d_1)}{8\mu_2(1-\nu_2)}\lambda d_3 \\ & + \frac{F_{M1}\exp(-\lambda d_2)}{8\mu_2\lambda M_1 M_2(1-\nu_2)}[-4\mu_2(1-\nu_2) \\ & (\mu_1(3-4\nu_2)(1-2\nu_1) - \mu_2(3-4\nu_1)(1-2\nu_2)) \\ & - M_1(\mu_1-\mu_2)(3-4\nu_2)\lambda d_3 + 2\lambda^2(\mu_1-\mu_2)M_1 sz], \\ \lambda U_{M1}(z) = {} & \frac{F_{M1}\exp(-\lambda d_1)}{8\mu_2(1-\nu_2)}(3-4\nu_2-\lambda d_1) + \frac{F_{M1}\exp(-\lambda d_2)}{8\mu_2 M_1 M_2(1-\nu_2)} \\ & [-2\lambda^2(\mu_1-\mu_2)M_1 zs + M_1(\mu_1-\mu_2)(3-4\nu_2)\lambda d_2 \\ & - (\mu_1^2(3-4\nu_2)^2 - \mu_2^2(3-4\nu_1)(5-12\nu_2+8\nu_2^2) \\ & + \mu_1\mu_2(3-4\nu_2)(2-4\nu_1)(1-2\nu_2))], \end{aligned} \tag{19}$$

$$\begin{aligned} T_{L1}(z)/\lambda = {} & \frac{F_{M1}\exp(-\lambda d_1)}{4(1-\nu_2)}(1-2\nu_2+\lambda d_1) \\ & + \frac{F_{M1}\exp(-\lambda d_2)}{4M_1 M_2(1-\nu_2)}[-2\mu_1^2(3-4\nu_2)(1-\nu_2) \\ & + 2\mu_2^2(3-4\nu_1)(1-\nu_2) + M_1(\mu_1-\mu_2)(3-4\nu_2) \\ & + M_1(\mu_1-\mu_2)(-\lambda s + \lambda z(3-4\nu_2) - 2\lambda^2 sz)], \\ T_{M1}(z) = {} & -\frac{F_{M1}\exp(-\lambda d_1)}{4(1-\nu_2)}\mathrm{sign}(z-s)(2-2\nu_2-\lambda d_1) \\ & + \frac{F_{M1}\exp(-\lambda d_2)}{4M_1 M_2(1-\nu_2)}[2\mu_1^2(3-4\nu_2)(1-\nu_2) \\ & - 2\mu_2^2(3-4\nu_1)(1-\nu_2) - M_1(\mu_1-\mu_2)(\lambda s \\ & + \lambda z(3-4\nu_2) - 2\lambda^2 sz)]. \end{aligned}$$

In these equations, we list results only for those terms corresponding to $m = 0$ and 1, signified by the subscripts 0 and 1, respectively. The terms corresponding to $m = -1$ can be obtained similarly.

6. Numerical results

In the limiting case, the Green's functions for a layered half-space can be verified by comparing them with Mindlin's solutions. In general, we consider a layered half-space (Fig. 3) composed of three layers with the elastic properties listed in Table 1. The layer interfaces are located at $z = 0.25$ and 1.5. It is noted that Case 1 in Table 1 corresponds to the Mindlin problem of a homogenous half-space.

We now compare two singularity extraction methods for this special case (Case 1). For brevity, we refer to the results obtained using Pan's algorithm [14], which makes use of the Kelvin solution, as Method I. The present approach, which employs the bi-material solution, is named Method II.

The objective is to obtain results of high accuracy corresponding to approximately six significant figures. However, the definition of error tolerance is complicated by computation of the displacements and stresses from the weighted sum of 15 integrals. Further, because it is not practical to establish apriori which, if any, of these integrals are predominant, failure of convergence in one or more integrals (which entails substantial computational cost) may not translate into significant loss of precision overall. To devise an algorithm which is both robust and (optimally) efficient under these conditions is difficult: we

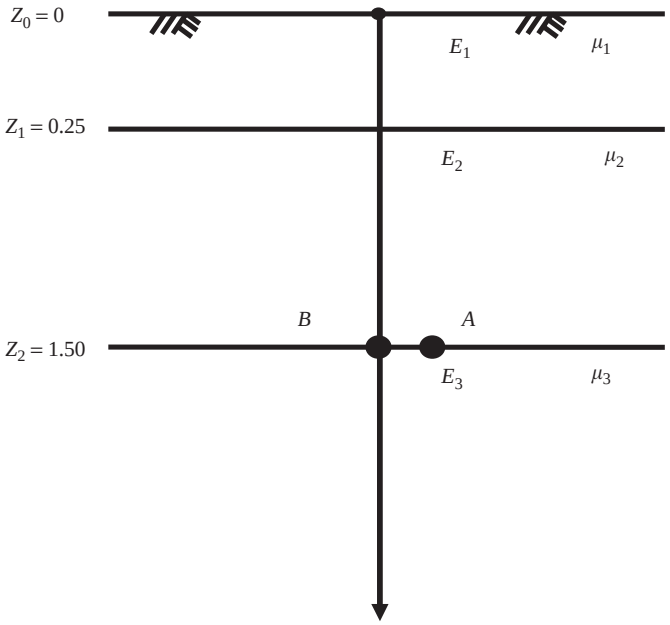

Fig. 3. Geometry of a three-layered half-space (not to scale).

Table 1
Elastic properties of a three-layered half-space

	Case 1		Case 2	
	E	v	E	v
Layer 1	1.0	0.25	1.0	0.25
Layer 2	1.0	0.25	5.0	0.25
Layer 3	1.0	0.25	25.0	0.25

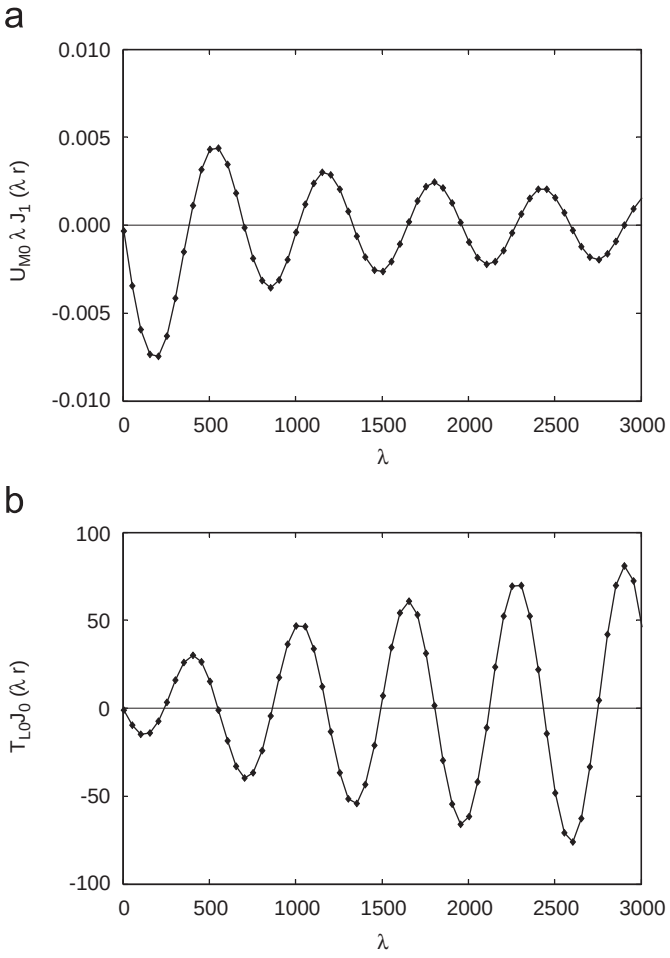

Fig. 4. Singular kernel functions: (a) $U_{M0}\lambda J_1(\lambda r)$ and (b) $T_{L0}J_0(\lambda r)$ for source point at B (0, 0, 1.5) and field point at A (0.01, 0, 1.5), corresponding to $r = 0.01$.

follow Pan [14] in adopting an algorithm, which delivers accurate results if it is convergent, but which may (or may not) deliver accurate results if convergence fails. The algorithm is therefore robust but not optimally efficient.

For non-singular cases, both methods converge and provide results with high precision (6S), but for near-singular cases (i.e., where the separation of the source and field points is an order of magnitude less than the layer thickness) convergence is much slower using Method I, as these points approach the free surface. This result is expected because it is well known that the Kelvin singular function differs from the Mindlin singular function by a factor of two (2), and therefore the singularity subtraction algorithm, using Method I, fails.

We now consider the more general problem in greater detail. A point source is located at (0, 0, 1.5), designated as point B: that is, on the interface between layers 2 and 3 (Fig. 3). Results are sought at a field point designated as point A (0.01, 0, 1.5), which is also located on the layer interface but at some small distance along the x-axis (Fig. 3). In relation to the characteristic dimensions of the problem (i.e., the layer thicknesses), this field point is near-singular. As noted above, in the numerical computation, 15 different numerical integrals must be computed to construct the layered Green's functions. Here we select from them kernel function 1, namely, $U_{M0}\lambda J_1(\lambda r)$, and kernel function 4, namely $T_{L0}J_0(\lambda r)$ for illustrative purposes. For field point A (i.e., $r = 0.01$), Fig. 4 shows how these kernel functions vary with λ: they are oscillatory and non-convergent over this range and consequently difficult to integrate. After subtraction of the singular part of the layered Green's function using the bi-material Green's function, the residues (non-singular parts of the layered Green's functions) present a very different picture, as shown in Fig. 5.

It is apparent from Fig. 5 that the residues are non-zero only near the origin, i.e., the residues converge quickly. Further, the magnitudes of these residues are only a small fraction of the corresponding singular parts. The non-zero values observed at large values of λ are spurious; these arise from numerical truncation errors. Some care is needed to ensure that these errors do not contaminate the solution, and this can be achieved by ensuring that the first integration interval is sufficiently small (i.e., less than the scaled first zero of the Bessel function).

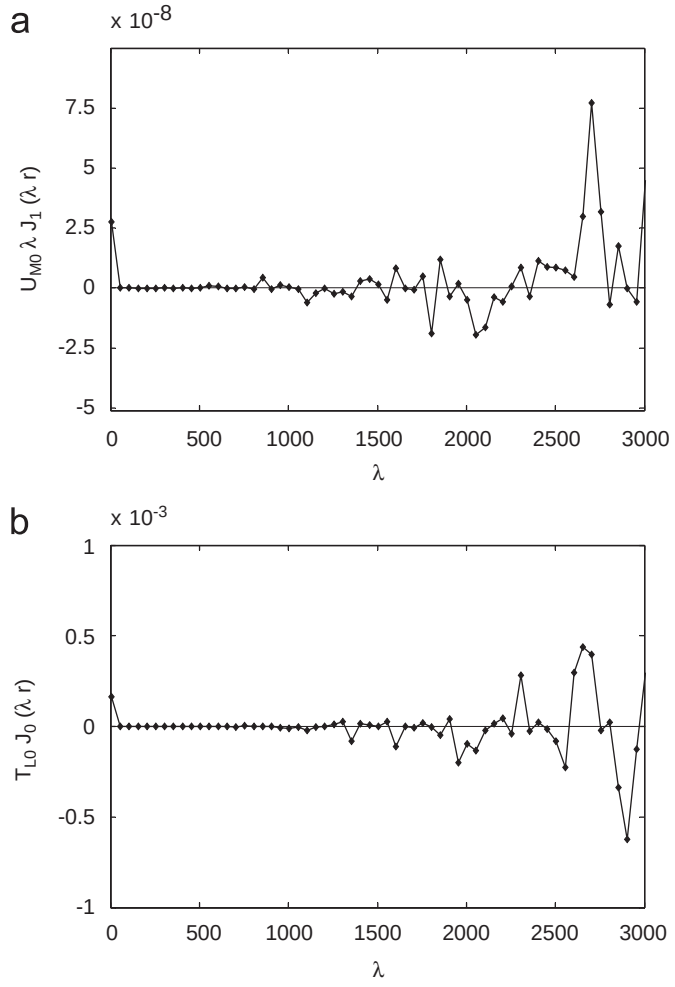

Fig. 5. Non-singular part of kernel functions: (a) $U_{M0}\lambda J_1(\lambda r)$, and, (b) $T_{L0}J_0(\lambda r)$ for source point at B (0, 0, 1.5) and field point at A (0.01, 0, 1.5), corresponding to $r = 0.01$.

Tables 2 and 3 list the displacements and stresses in the three-layered half-space, using the singular extraction Method I (full space) and Method II (bi-material) resulting from unit point forces directed along the three axes (x, y and z, respectively).

We observe from Table 2 the excellent agreement, for displacements, between the two methods. However, the results obtained by Method II require only a small fraction (less than 5%) of the computational time taken by Method I, because Method I (unlike Method II) fails to converge. This failure of convergence of Method I is significant here as may be observed by comparing the corresponding stresses in Table 3. These show that, in most cases, three significant figure accuracy is the best that can be achieved using Method I, and only then by expending considerably more (at least one order of magnitude) computational effort.

This result can be traced to the failure of the singularity subtraction method, using Method I, at the interface between two dis-similar materials, which consequently necessitates numerical integration of singular kernel functions similar to those depicted in Fig. 4, rather than those in Fig. 5.

Fig. 6 illustrates the variation along the x-axis on the interface between layers 2 and 3 (i.e., on the plane $z = 1.5$) of, (a), vertical displacement u_z^z and, (b), shear stress σ_{xz}^z due to a vertical point force at (0, 0, 1.5), for the two cases listed in Table 1: namely a 3-layered material and a homogenous material. The singularity is captured in both cases using the bi-material singular extraction method (i.e., Method II). The relatively soft 3-layered material undergoes significantly greater deformation than the homogenous material, but the shear stress distributions are very similar.

Table 2
Displacements at field point A (0.01, 0, 1.5) due to unit point force at B (0, 0, 1.5)

	Due to unit point force F_x		Due to unit point force F_y		Due to unit point force F_z	
	Method I (full-space)	Method II (bimaterial)	Method I (full-space)	Method II (bimaterial)	Method I (full-space)	Method II (bimaterial)
u_x	1.3273456	1.3273458	0.0	0.8 E-16	−0.2066951	−0.2066952
u_y	0.0	0.0	0.93118093	0.93118091	0.0	0.0
u_z	0.2066954	0.2066952	0.0	0.1 E-16	0.9325203	0.9325200

Table 3
Stresses at field point A (0.01, 0, 1.5) due to unit point force at B (0, 0, 1.5)

	Due to unit point force F_x		Due to unit point force F_y		Due to unit point force F_z	
	Method I (full-space)	Method II (bimaterial)	Method I (full-space)	Method II (bimaterial)	Method I (full-space)	Method II (bimaterial)
σ_{xx}	−603.2	−602.8	0.0	−0.3 E-13	82.64	82.67
σ_{yy}	86.3	86.1	0.0	0.5 E-14	−82.72	−82.69
σ_{zz}	155.3	155.0	0.0	0.9 E-14	−0.14	−0.02
σ_{yz}	0.0	0.0	34.4	34.5	0.0	0.0
σ_{xz}	−34.9	−34.4	0.0	−0.2 E-14	−154.9	−155.0
σ_{xy}	0.0	0.0	−106.793	−106.792	0.0	0.0

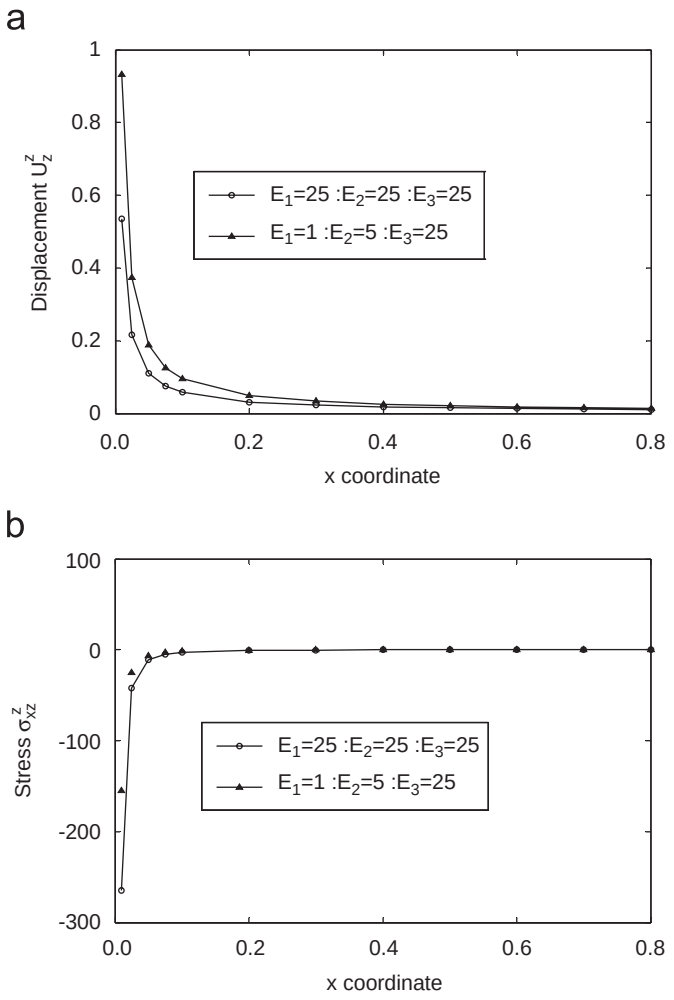

Fig. 6. Interface profile along x-axis of: (a) vertical displacement, u_z^z and (b) shear stress σ_{xz}^z.

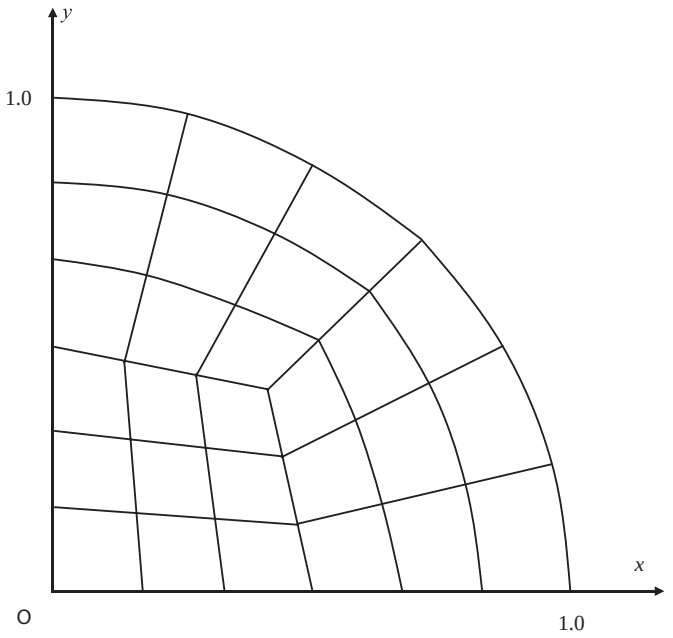

Fig. 7. Boundary element mesh for disk foundation.

To illustrate the application of these Green's functions to boundary element analysis, we analyze the settlement of a smooth (frictionless) flexible disk of unit radius R subjected to unit vertical pressure and founded on a three-layered halfspace, defined by the material properties of Table 1 (Case 2) and the geometry of Fig. 3. Making use of quadrantal symmetry, 33 eight-noded quadratic boundary elements (Fig. 7) are used to discretize the disk: the free-surface condition is automatically satisfied. The results of the analysis (Fig. 8), obtained by using the three-dimensional code, BEMECH [29] show: (a) the settlement profile of the ground surface and (b) the variation of vertical displacement with depth below the disk centroid. On this scale, the results are indistinguishable from a corresponding multi-region analysis [30] using Kelvin's solution for each region which requires a total of 324 elements: outside the disk, the infinite surface is truncated at a radius of 50 units and discretized using just 8 quadratic boundary elements in the radial direction, while layer 3 is assumed to be underlain by a rigid layer at a depth z of 6 units. This analysis yields a centroidal surface settlement, which is 0.8% greater than that obtained using the multi-layer Green's functions. Also shown in Fig. 8 for comparison purposes are the analytical settlement profiles for a homogenous half-space (normalized to the same centroidal surface settlement). Fig. 8(a) shows that surface settlements decay very rapidly outside the loaded area for the multi-layered half-space by comparison with the homogenous half-space, while the profile of vertical settlements with respect to depth beneath the centroid (Fig. 8(b)) clearly reflects the stiffness profile itself, i.e., settlements are concentrated in the more compliant upper layers. In this simple example, despite the substantial reduction in the number of boundary elements, the saving in computational time resulting from use of the multi-layer Green's functions is not significant. However, the advantages of reduced data preparation effort; the ability to cope effectively with difficult geometries (i.e., very thin layers) and the scope for further significant computational efficiency gains (including specification of less stringent error tolerances) offers considerable promise.

7. Conclusion

Some of the difficulties of computing three-dimensional Green's functions in multi-layered half-spaces have been explored. This investigation shows that a significant gain in computational efficiency and accuracy can be obtained by utilizing the closed-form solutions for the bi-material half-space. A boundary element analysis illustrates the potential of this approach in practical multi-layered problems, where accurate efficient computation of near-singular kernel functions is of paramount importance.

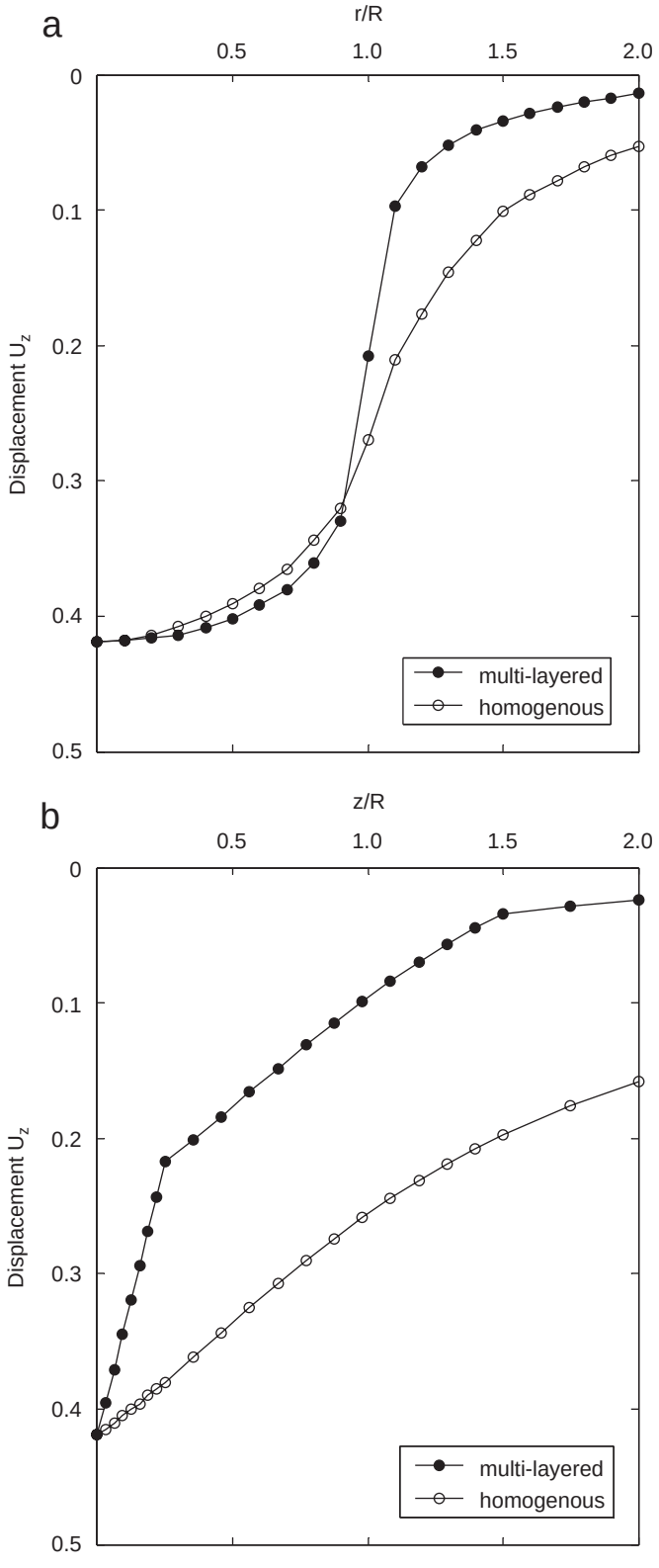

Fig. 8. Vertical displacements due to disk loading: (a) along the ground surface and (b) beneath the disk centroid.

References

[1] Thomson WT. Transmission of elastic waves through a stratified medium. J Appl Phys 1950;21:89–93.

[2] Haskell A. The dispersion of surface waves on a multilayered media. Bull Seism Soc Am 1953;43:17–34.

[3] Gilbert F, Backus G. Propagator matrices in elastic wave and vibration problems. Geophysics 1966;31:326–32.

[4] Kausel E, Peek R. Dynamic loads in the interior of a layered stratum: an explicit solution. Bull Seismol Soc Am 1982;72:1459–81.

[5] Luco JE, Apsel RJ. On the Green's functions for a layered half-space. Part I. Bull Seismol Soc Am 1983;73:909–29.

[6] Franssenns GR. Calculation of the elastodynamic Green's function in layered media by means of a modified propagator matrix method. Geophys J R Astr Soc 1983;75:669–91.

[7] Bouden M, Khair KR, Datta SK. Ground motion amplification by cylindrical valleys embedded in a layered medium. Earthquake Eng Struct Dynam 1990;19:497–512.

[8] Singh SJ. Static deformation of a multilayered half space by internal sources. J Geophys Res 1970;75:3257–63.

[9] Jovanovich DB, Husseini MI, Chinnery MA. Elastic dislocations in a layered half-space—I. Basic theory and numerical methods. Geophys J R Astro Soc 1974;39:205–17.

[10] Sato R, Matsu'ura M. Static deformations due to fault spreading over several layers in a multi-layered medium, part I: displacement. J Phys Earth 1973;21:227–49.

[11] Singh SJ. Static deformation of a transversely isotropic multi-layered half-space by surface loads. Phys Earth Planet Inter 1986;42:263–73.

[12] Yue ZQ, Wang R. Static solution for transversely isotropic elastic *n*-layered system. Acta Sci Nat Univ Pekinensis 1988;24:202–11.

[13] Chan KS, Karasudhi P, Lee SL. Force at a point in the interior of a layered half-space. Int J Solids Struct 1974;10:1179–99.

[14] Pan E. Static Green's functions in multilayered half spaces. Appl Math Modell 1997;21:509–21.

[15] Pan E. Static response of a transversely isotropic and layered half-space to general surface loads. Phys Earth Planet Inter 1989;54:353–63.

[16] Pan E. Static response of a transversely isotropic and layered half-space to general dislocation sources. Phys Earth Planet Inter 1989;58:103–17.

[17] Yuan FG, Yang B. Three-dimensional Green's functions for composite laminates. Int J Solids Struct 2003;40:331–42.

[18] Yang B, Pan E. Efficient evaluation of three-dimensional Green's functions in anisotropic elastostatic multilayered composites. Eng Anal Boundary Elements 2002;26:355–66.

[19] Yang B, Pan E. Three-dimensional Green's functions in anisotropic trimaterials. Int J Solids Struct 2002;39:2235–55.

[20] Guzina BB, Pak RYS. On the analysis of wave motions in a multi-layered solid. Q J Mech Appl Math 2001;54:13–37.

[21] Patterson TNL. The optimum addition of points to quadrature formulae. Math. Comp. 1968;22:847–56.

[22] Patterson TNL. Algorithm for automatic numerical integration over a finite interval. Commun ACM 1973;16:694–9.

[23] Chave AD. Numerical integration of related Hankel transforms by quadrature and continued fraction expansion. Geophysics 1983;48:1671–86.

[24] Hanggi P, Roesel F, Trautmann P. Evaluation of infinite series by use of continued fraction expansions: a numerical study. J Comp Phys 1980;37:252–8.

[25] Pan YC, Chou TW. Green's function solutions for semi-infinite transversely isotropic materials. Int J Eng Sci 1979;17:545–51.

[26] Yue ZQ. Closed-form Green's functions for transversely isotropic bi-solids with a slipping interface. Struct Eng Mech 1996;4:469–84.

[27] Guzina BB, Pak RYS. Static fundamental solutions for a bi-material full-space. Int J Solid Struct 1999;36:493–516.

[28] Xu J. Boundary element analysis of stratified ground. PhD. thesis, Glasgow University, UK, 2007.

[29] Gao XW, Davies TG. Boundary element programming in mechanics. New York: Cambridge University Press; 2002.

[30] Gao XW, Davies TG. 3D multi-region BEM with corners and edges. Int J Solid Struct 2000;37:1549–60.